ARMA 20–1762

Characterizing Fault Zone Structure and Geometry using Photogrammetry and 3D Geologic Modeling

Krajnovich, A., Zhou, W. and Gutierrez, M.

Colorado School of Mines, Golden, Colorado, USA

This paper was prepared for presentation at the 54th US Rock Mechanics/Geomechanics Symposium held in Golden, Colorado, USA, 28 June-1 July 2020. This paper was selected for presentation at the symposium by an ARMA Technical Program Committee based on a technical and critical review of the paper by a minimum of two technical reviewers. The material, as presented, does not necessarily reflect any position of ARMA, its officers, or members. Electronic reproduction, distribution, or storage of any part of this paper for commercial purposes without the written consent of ARMA is prohibited. Permission to reproduce in print is restricted to an abstract of not more than 200 words; illustrations may not be copied. The abstract must contain conspicuous acknowledgement of where and by whom the paper was presented.

ABSTRACT: In nature, faults rarely occur as discrete slip surfaces but instead as zones of fractured and displaced rock centered around an approximate central fault surface. These fault zones introduce altered geotechnical strength and hydraulic permeability to the surrounding rockmass, making their characterization important to geotechnical engineering projects such as hard rock tunneling. Inherent heterogeneity of the fault zone composition is common, with synthetic (parallel to fault zone) and antithetic (perpendicular to fault zone) faults producing a complex internal fracture network. This heterogeneity results in subjectivity when defining the boundaries of fault zone components such as the damage zone and fault core. This study demonstrates a semi-automatic, quantitative workflow for characterizing the fracture network comprising a fault zone focusing on assessing the network geometry using principal fracture sets and the rockmass structure using areal fracture density. In an outcrop study of fault zones above the Eisenhower-Johnson Memorial Tunnels (EJMT) in Colorado, USA, point clouds derived from unmanned aerial vehicle (UAV) photogrammetry were collected over historically mapped fault zones. These data are used in accordance with prior knowledge on the nature of fault zones in the project locality to quantitatively characterize the fault zone internal structure and geometry.

1. INTRODUCTION

Widespread access to high-resolution, photogrammetric point cloud data and the ongoing development of open source point cloud processing software programs have created a unique opportunity for enhancing site characterization projects in geological engineering (Buyer et al., 2020; Fekete & Diederichs, 2013; Ferrero et al., 2009), structural geology (Thiele et al., 2019) and reservoir modelling (Bisdom et al., 2017).

A variety of tools have been developed in specific fields (e.g., block analysis, fracture network connectivity) providing a diverse toolset that have been synthesized into a workflow for analyzing the structure and geometry of the fracture network comprising a fault zone (i.e., the zone of fractured and/or displaced rock surrounding a fault surface). In the context of this work, the term ‘geometry’ refers to the orientation and nature of the principal fracture surfaces, while the term ‘structure’ refers to numerical characteristics of the rockmass such as fracture intensity.

The methodology proposed in this paper synthesizes recent research into semi-automatic identification and classification of rockmass discontinuities from photogrammetric data focusing on two related rockmass characteristics: discontinuity surfaces (Discontinuity Set Extractor by Riquelme et al., 2014) and discontinuity traces (NetworkGT Toolbox by Nyberg et al., 2018; Automatic Fracture Detection Code by Prabhakaran et al., 2019). While not yet a replacement for traditional field investigations, this work displays the potential of photogrammetric analysis of rockmasses to provide robust datasets for addressing classical problems in geological characterization. Powerful visualization is enabled using GIS and 3D geologic modeling software (ArcMap and Leapfrog Works) to provide a comprehensive view of the rockmass characteristics while also allowing for future incorporation in subsurface modeling.

The Eisenhower-Johnson Memorial Tunnels (EJMT) in Colorado, USA, constructed in the 1960s-1970s (Robinson et al., 1974), are 1.6 mile, twin roadway tunnels excavated through uplifted crystalline rocks of the Rocky Mountains. The tunnel alignment crosses a number of fault zones in the subsurface believed to be associated with the nearby regional Loveland-Berthoud Pass fault zone. A number of these fault zones were mapped at the

surface by Robinson et al., 1974, prompting a recent series of field mapping outings in 2018-2019 using an unmanned aerial vehicle (UAV) to capture photogrammetric data. The acquired dataset provides a platform for applying the proposed methodology to reveal additional information on the fault zones.

2. METHODOLOGY

Headwall 4, the chosen outcrop for photogrammetric mapping, is shown in Figure 1 alongside the flight boundary and the geologic map of Robinson et al., 1974. Flight planning was performed using the DroneDeploy application and images were collected using a DJI Mavic 2 Zoom drone. The site geology consists of a 10 meter high outcrop of the Silver Plume Granite (SPG), intersecting two mapped fault zones (trending N-S and NW-SE). The site was also chosen based on the abundance of clear fracture surfaces and traces visible. Nine ground control points were laid out across the breadth and height of the outcrop for use in processing the UAV images using the Structure from Motion (SfM) method in Agisoft Metashape.

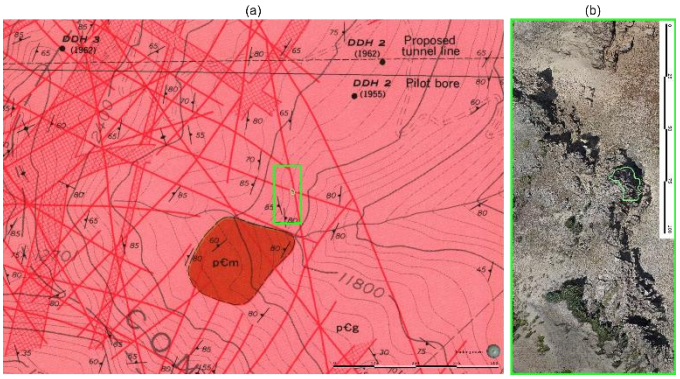

Figure 1. Regional geologic map by Robinson et al., 1974 with Headwall 4 boundary shown in green (a), and 3D point cloud data with the interpretation boundary shown in light green (b).

The workflow shown in Figure 2 represents the primary workflow for analyzing the point cloud data acquired via photogrammetry. The data are exported in 3D point cloud format and as a georeferenced orthophoto. These data are fed into the two respective processing methods: surface-based and image-based analysis. Surface-based analysis has been popularized by recent works in geological engineering focusing on rockmass characterization and rockfall analysis, while image-based trace analysis has been popularized by ongoing work in reservoir engineering focusing on fracture network connectivity. Prior to analysis, the point cloud data are visualized and explored using software such as Maptek I-Site Studio and CloudCompare.

2.1. Surface-based Analysis

The goal of surface-based analysis is to classify the fracture surfaces present in the point cloud data based on shared orientations. The classified point cloud is then compared to expected fracture orientations for analysis. Optional point cloud cleaning should be performed prior to classification to remove incoherent points (e.g., excessive vegetation, processing artifacts). The Discontinuity Set Extractor (DSE) software is a semi-automatic method for identifying, classifying and extracting the fracture sets present in a point cloud. The parameters used in DSE are in Table 1 and the interested reader is referred to Riquelme et al., 2014 for more detailed information.

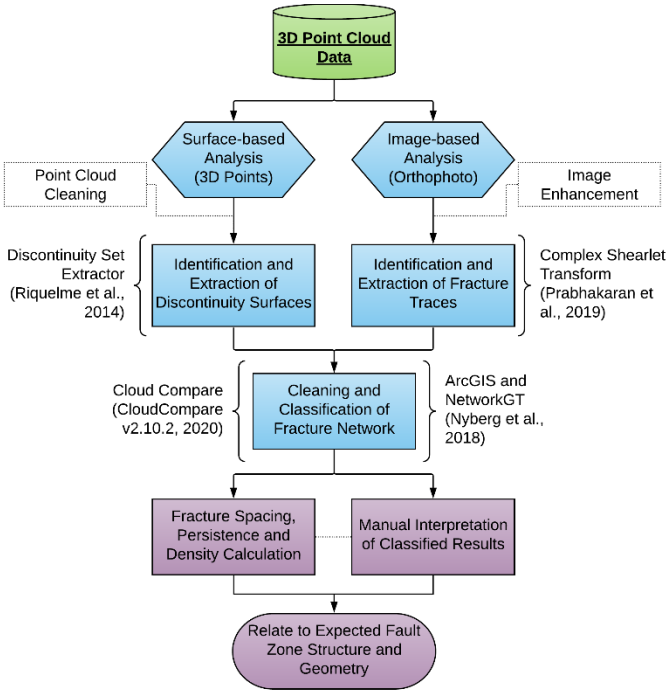

Figure 2. Developed workflow for assessing fault zone structure and geometry using open source codes to perform surface-based and image-based analysis of photogrammetric point cloud data.

Table 1. Parameters used in DSE.

Parameter	Value
knn	30 (default)
eta	0.2 (default)
n_bins	64 (default)
angle_v_ppal	22
cone	30
# discontinuity sets	8
k_sigma	1.5 (default)

2.2. Image-based Analysis

The purpose of image-based analysis is extracting lines describing fracture traces present on the outcrop. In a

similar process to surface-based analysis, the fracture traces are classified based on orientation and compared to the expected fracture orientations. Enhancing the orthophoto product using a photo editing software can greatly improve fracture trace detection for outcrops with variable light conditions (i.e., shadows). The complex shearlet transform method of automatic fracture detection produced by Prabhakaran et al., 2019 is an advanced method for fracture trace identification from digital images. The published method is calibrated for UAV images and requires as input the pixel size of the image (maximum size: 1000x1000) and a threshold parameter that controls the balance accurate fracture detection and background noise. The threshold parameter was chosen to be 0.62 based on visual analysis.

2.3. Cleaning

Following the processing and classification of the point cloud data, the initial results must be cleaned and repaired to improve the ability to extract relevant fracture network characteristics. For bot classification methods, manual editing typically involves deleting small insignificant surfaces and traces. Additionally, for the extracted fracture network traces the NetworkGT toolbox (Nyberg et al., 2018) provides a useful tool for 'repairing' the fracture network polylines by joining nearby fractures. Due to the inherent noise present when using semi-automatic classification techniques, this step of inspection and cleaning is critical to enhance the ability to visualize and characterize the rockmass structure and geometry. The parameters used during automatic detection and classification were manipulated through several exploratory analyses to minimize the level of manual editing required. The results presented in this study adhere to a goal of minimizing detailed manual manipulations of the point cloud data and processed results, exhibiting the strengths and limitations of relying on semi-automatic processing workflows for geologic characterization.

3. RESULTS

An interpretation boundary was defined for a chosen section of the study area (Figure 3(a)) to focus the analysis on a representative area of the outcrop. The chosen area contains a mixture of visible fracture surfaces and fracture traces of varying orientations and is intersected by historically mapped two fault zones. The classified results based on expected synthetic and antithetic fault surfaces of the two mapped fault zones are shown in Figures 3(b-c) for fracture surfaces and traces respectively.

The primary analysis of processed results was performed in ArcGIS. The GIS software allowed for adding additional classification attributes to the fracture traces and surfaces within the interpretation boundary, such as joint set numbers, trace lengths and areal statistics. Combined with the NetworkGT toolbox, ArcGIS is a

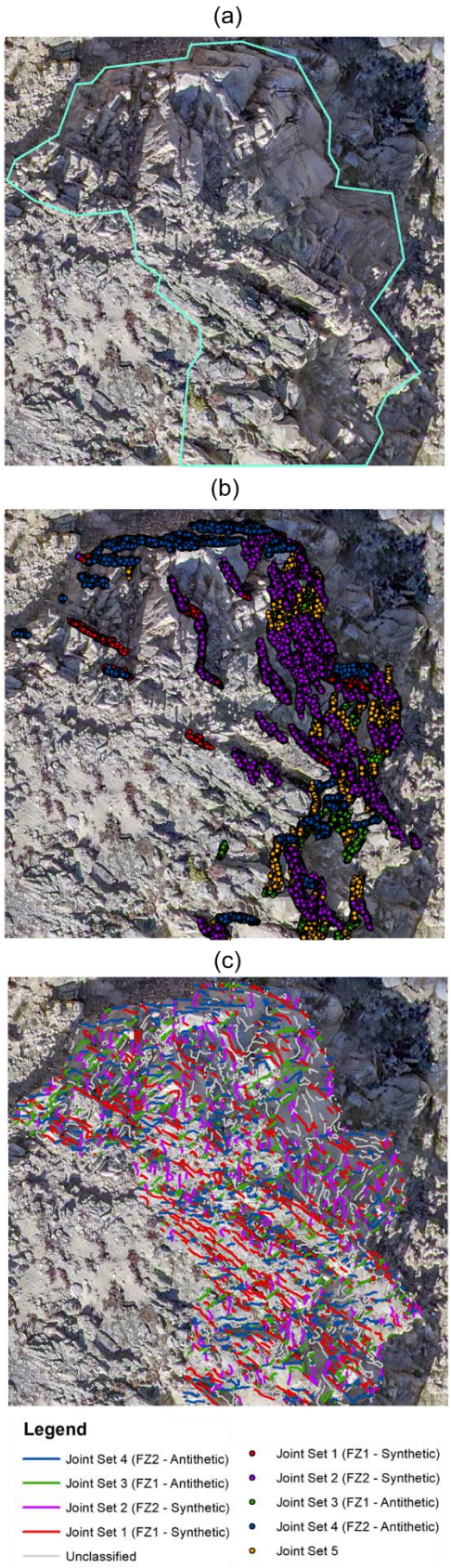

Figure 3. Extracted section of point cloud data after image enhancement showing interpretation boundary (a), classified fracture surface points (b) and classified fracture traces (c).

powerful tool for performing spatial analysis on the processed point cloud results.

The fault zones intersecting the interpretation boundary are fault zone 1 (FZ1) oriented at 285˚ and fault zone 2 (FZ2) oriented at 345˚. Fracture sets were defined in the processed results to highlight the planes and traces oriented parallel to each fault zone (i.e., synthetic faults) and the surfaces and traces oriented perpendicular to each fault zone (i.e., antithetic faults). This classification (Figure 4) respects published literature on the internal geometry of fault zones (Childs et al., 2009; Kim et al., 2004) while also reducing the amount of irrelevant data contributing to fault zone characterization. Fracture sets were given a tolerance of 30˚ for classifying fracture surfaces and 15˚ for classifying fracture traces.

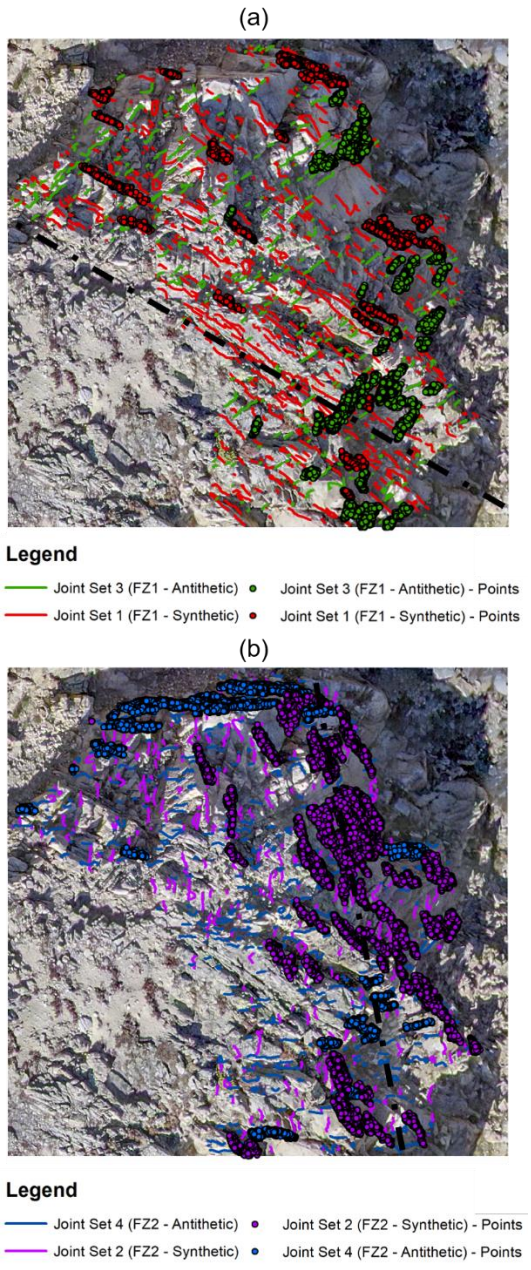

Figure 4. Extracted fracture surfaces and traces interpreted as representing synthetic and antithetic faults of FZ1 (a) and FZ2 (b).

The primary tool for characterizing the fault zone structure is the P_{21} value (areal fracture density), calculated from the fracture trace data onto a 1 meter grid in ArcGIS (Figure 5). The calculation was performed using several different combinations of fracture set orientations including all fracture traces, synthetic fault traces only, and combined synthetic and antithetic fault traces. The different binning strategies were employed to overcome noise in the data due to imperfect outcrop conditions and the semi-automatic trace detection algorithm.

(a) Summary Statistics

Fracture Network	Mean (P_{21})	STD (P_{21})
(a) All Fractures	4.98	1.73
(b) FZ1 – Synthetic	1.23	0.79
(c) FZ1 – Synthetic and Antithetic	1.73	0.91
(d) FZ2 – Synthetic	0.72	0.50
(e) FZ2 – Synthetic and Antithetic	1.40	0.71

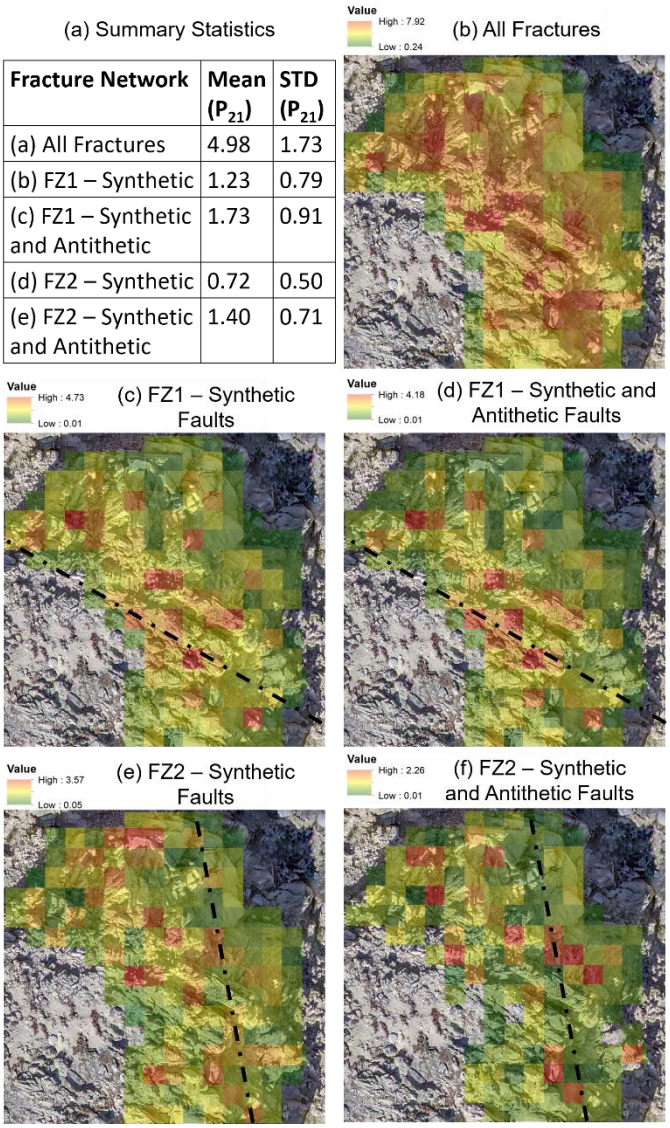

Figure 5. Summary statistics of P_{21} values calculated on a 1 meter grid over the interpretation boundary (a) for all fractures (b), synthetic faults of FZ1 and FZ2 (c,e) and synthetic and antithetic faults of FZ1 and FZ2 (d,f).

The P_{21} results show a concentration of fractures about the approximate centerline of FZ1 and not for FZ2. The effect of noise in the fracture trace identification and classification is apparent. Particularly, upon visual inspection several high P_{21} pixels contain overlying rocks on the rockmass which contribute additional, false fractures. The boundaries of the P_{21} concentration also

roughly coincide with the outcrop's boundaries with overburden, suggesting that the true P_{21} distribution of the rockmass may not be accurately conveyed.

Accompanying P_{21} calculation from fracture traces, the distribution of fracture spacing in 3D space can be calculated from the fracture surfaces (Riquelme et al., 2015). The computed normal spacing from 3D surfaces was compared to normal spacing of FZ1 synthetic fault traces taken from 6 parallel scanlines considering the 3D distance between scanline fracture intersections (Figure 6). The average calculated spacings are in relatively close agreement (0.70 m and 1.05 m) and cover similar ranges.

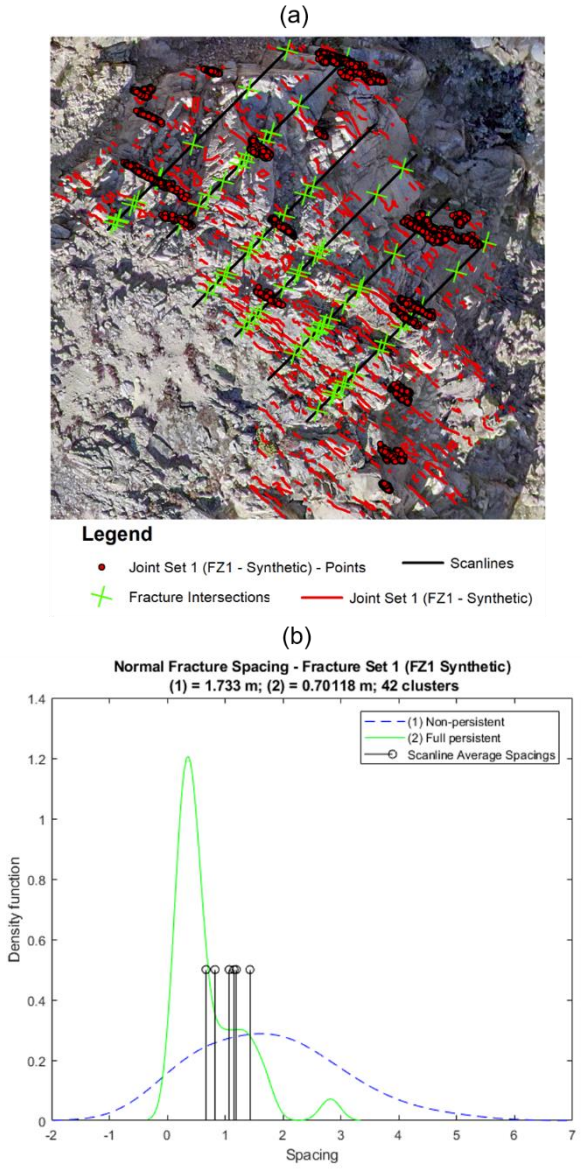

Figure 6. Calculated normal fracture spacings for FZ1 synthetic faults computed over six scanline intersections (a) and from the classified 3D point cloud in DSE (b).

4. DISCUSSION

The differing coverage and sensitivity to fracture orientations of the fracture trace and fracture surface detection algorithms are apparent. The most significant difference is illustrated in Figure 7 where the coverage of the fracture surface detection algorithm is heavily concentrated about the cliff face, failing to characterize the fracture sets present on the upper portion of the outcrop. Furthermore, the majority of the discontinuity surface orientations are normal to the outcrop surface, suggesting that a 3D effect is contributing to the observed surface orientations. In this context, the 3D effect is akin to the concept of apparent dip, where the combined angle of a fracture surface with the angle of the outcrop surface can skew the distribution of observed fracture orientations.

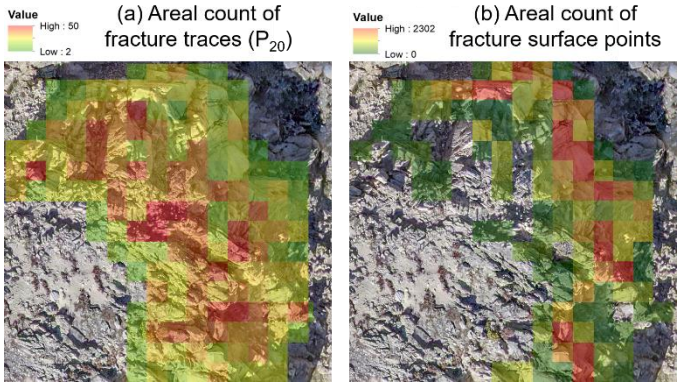

Figure 7. Differing coverage of fracture trace and fracture surface detection shown by the areal fracture intensity (P_{20}) (a) and the areal count of fracture surface points (b).

However, as evidenced by the analysis performed in this work, both methods have strengths and limitations and when utilized in tandem, the ability to characterize fracture network structure and geometry can be improved. There are several reasons for this improvement, all stemming from the base concept that the fracture surfaces and fracture traces are data describing the same, real world fracture network. In particular, different sections of the rockmass may be more or less dominated by fracture surfaces or by fracture traces (Figure 7). Additionally, fracture sur]-faces may be more prone to changes in geometry due to weathering and erosion than fracture traces are. The proposed workflow currently allows for the direct comparison of extracted fracture set orientations and normal spacings and can be expanded in the future to incorporate additional quantitative comparisons between the point and trace data products.

Several limitations of the approach were identified, primarily the issues of over classification and misclassification. The presence of overlying rocks and strong shadows on the outcrop leads to spurious over classification of fracture surfaces and traces. While these over classifications do not heavily influence visual interpretation of the classified results, their presence does influence the calculation of P_{21} values leading to apparent overestimation. Misclassification arose in two major forms in the proposed workflow: splitting of persistent

fractures between two fracture sets and incorrect binning of fracture traces. Regarding both fracture surfaces and traces, the semi-automatic classification algorithms can result in continuous fracture surfaces being split between classifications due to their angular proximity to neighboring fracture sets. Incorrect binning of fracture traces is believed to occur due to the complex shapes of certain fracture traces (e.g., J or L shaped fracture polylines) which limits the NetworkGT toolbox's ability to correctly assign set orientations. Both limitations can be seen in Figure 3(b)-(c).

The outcrop studied with the proposed workflow suffers from non-ideal conditions for fracture mapping including the presence of overburden and heavy surficial weathering. While the effects of these conditions are apparent in the processed results (e.g., over classification of fracture traces and 3D effect on fracture surfaces), the proposed workflow proved to be robust, able to extract valuable information such as synthetic and antithetic fault surfaces, fracture spacings and areal fracture density values.

5. CONCLUSIONS

The proposed semi-automatic workflow produces a realistic characterization of fault zone structure (fracture density) and geometry (principal fracture set orientations) in the studied outcrop section. The issues discussed highlighted the key limitations of the method including the presence of noise, misclassifications and overestimation of joint density due to misidentification of fracture traces. Inherent complexity of the mapped fault zones compounded by these issues requires experienced interpretation of the data to determine whether or not meaningful features are present in the data.

The fracture network geometry matched the expected geometry of the known fault zones and their components (FZ1 and FZ2, synthetic and antithetic faults) despite the high noise levels, while the P21 calculation was more heavily influenced by noise levels.

6. FUTURE WORK

Future work will focus on verification of the semi-automatic processing results by manual mapping comparison, conducted both on the point cloud data directly and in the field using traditional mapping methods. Additional manual intervention in modifying the open source algorithms used is possible, for example expanding the fracture detection code of Prabhakaran et al., 2019 to automate over larger images, or modifying the way in which NetworkGT assigns fracture set orientations to complex shaped traces to reduce misclassification. Applying the workflow to other outcrops containing suspected fault zones will further test the robustness of the proposed methodology. Finally, incorporating the processed results into subsurface modeling by way of 3D geologic modeling or discrete fracture network modeling presents a novel way to expand the usefulness of the method. This additional modeling could open new avenues for improving the relationship and interoperability of fracture trace and fracture surface products.

7. ACKNOWLEDGEMENTS

Support from the University Transportation Center for Underground Transportation Infrastructure (UTC-UTI) at the Colorado School of Mines for funding this research under Grant No. 69A3551747118 from the U.S. Department of Transportation (DOT) and Colorado DOT PO number 471001372 is gratefully acknowledged. Additional support from Maptek through the provision of access to the PointStudio software is gratefully acknowledged. The authors also wish to acknowledge the staff at Loveland Ski Area for allowing and supporting multiple field work visits. Finally, the other members of the EJMT research group are gratefully acknowledged for their contributions to the success of the field trips including Gauen Alexander, Hui Lu, Jacob Mellema and Colum Marshall.

REFERENCES

Bisdom, K., Nick, H. M., & Bertotti, G. (2017). An integrated workflow for stress and flow modelling using outcrop-derived discrete fracture networks. *Computers and Geosciences*, *103* (November 2016), 21–35. https://doi.org/10.1016/j.cageo.2017.02.019

Buyer, A., Aichinger, S., & Schubert, W. (2020). Applying photogrammetry and semi-automated joint mapping for rock mass characterization. *Engineering Geology*, *264* (July 2019). https://doi.org/10.1016/j.enggeo.2019.105332

Childs, C., Manzocchi, T., Walsh, J. J., Bonson, C. G., Nicol, A., & Schöpfer, M. P. J. (2009). A geometric model of fault zone and fault rock thickness variations. *Journal of Structural Geology*, *31*(2), 117–127. https://doi.org/10.1016/j.jsg.2008.08.009

Fekete, S., & Diederichs, M. (2013). Integration of three-dimensional laser scanning with discontinuum modelling for stability analysis of tunnels in blocky rockmasses. *International Journal of Rock Mechanics and Mining Sciences*, *57*, 11–23. https://doi.org/10.1016/j.ijrmms.2012.08.003

Ferrero, A. M., Forlani, G., Roncella, R., & Voyat, H. I. (2009). Advanced geostructural survey methods applied to rock mass characterization. *Rock Mechanics and Rock Engineering*, *42*(4), 631–665. https://doi.org/10.1007/s00603-008-0010-4

Kim, Y. S., Peacock, D. C. P., & Sanderson, D. J. (2004). Fault damage zones. *Journal of Structural Geology*,

26(3), 503–517. https://doi.org/10.1016/j.jsg.2003.08.002

Nyberg, B., Nixon, C. W., & Sanderson, D. J. (2018). NetworkGT: A GIS tool for geometric and topological analysis of two-dimensional fracture networks. *Geosphere*, *14*(4), 1618–1634. https://doi.org/10.1130/GES01595.1

Prabhakaran, R., Bruna, P.-O., Bertotti, G., & Smeulders, D. (2019). An automated fracture trace detection technique using the complex shearlet transform. *Solid Earth Discussions*, 1–40. https://doi.org/10.5194/se-2019-104

Riquelme, A. J., Abellán, A., & Tomás, R. (2015). Discontinuity spacing analysis in rock masses using 3D point clouds. *Engineering Geology*, *195*, 185–195. https://doi.org/10.1016/j.enggeo.2015.06.009

Riquelme, A. J., Abellán, A., Tomás, R., & Jaboyedoff, M. (2014). A new approach for semi-automatic rock mass joints recognition from 3D point clouds. *Computers and Geosciences*, *68*, 38–52. https://doi.org/10.1016/j.cageo.2014.03.014

Robinson, C. S., Lee, F. T., Scott, J. H., Carroll, R. D., Hurr, R. T., Richards, D. B., … Abel, J. F. (1974). *Engineering Geologic, Geophysical, Hydrologic, and Rock-Mechanics Investigations of the Straight Creek Tunnel Site and Pilot Bore, Colorado*. *USGS Numbered Series 815*. Washington, D.C.: United States Government Printing Office. https://doi.org/10.3133/pp815

Thiele, S. T., Grose, L., Cui, T., Cruden, A. R., & Micklethwaite, S. (2019). Extraction of high-resolution structural orientations from digital data: A Bayesian approach. *Journal of Structural Geology*, *122*, 106–115. https://doi.org/10.1016/j.jsg.2019.03.001